eScholarship@UMassChan

Shelterin components mediate genome reorganization in response to replication stress

Item Type	Journal Article
Authors	Mizuguchi, Takeshi;Taneja, Nitika;Matsuda, Emiko;Belton, Jon-Matthew;FitzGerald, Peter;Dekker, Job;Grewal, Shiv I. S
Citation	Proc Natl Acad Sci U S A. 2017 May 23;114(21):5479-5484. doi: 10.1073/pnas.1705527114. Epub 2017 May 10. Link to article on publisher's site
DOI	10.1073/pnas.1705527114
Rights	Publisher PDF posted as allowed by the publisher's author rights policy at http://www.pnas.org/site/aboutpnas/authorfaq.xhtml.
Download date	2024-12-26 01:43:22
Link to Item	https://hdl.handle.net/20.500.14038/49836

Shelterin components mediate genome reorganization in response to replication stress

Takeshi Mizuguchi[a,1], Nitika Taneja[a], Emiko Matsuda[a], Jon-Matthew Belton[b], Peter FitzGerald[c], Job Dekker[b], and Shiv I. S. Grewal[a,2]

[a]Laboratory of Biochemistry and Molecular Biology, National Cancer Institute, National Institutes of Health, Bethesda, MD, 20892; [b]Howard Hughes Medical Institute, Program in Systems Biology, Department of Biochemistry and Molecular Pharmacology, University of Massachusetts Medical School, Worcester, MA 01605; and [c]Genome Analysis Unit, National Cancer Institute, National Institutes of Health, Bethesda, MD 20892

Contributed by Shiv I. S. Grewal, April 5, 2017 (sent for review December 30, 2016; reviewed by Steven E. Jacobsen and Nevan J. Krogan)

The dynamic nature of genome organization impacts critical nuclear functions including the regulation of gene expression, replication, and DNA damage repair. Despite significant progress, the mechanisms responsible for reorganization of the genome in response to cellular stress, such as aberrant DNA replication, are poorly understood. Here, we show that fission yeast cells carrying a mutation in the DNA-binding protein Sap1 show defects in DNA replication progression and genome stability and display extensive changes in genome organization. Chromosomal regions such as subtelomeres that show defects in replication progression associate with the nuclear envelope in *sap1* mutant cells. Moreover, high-resolution, genome-wide chromosome conformation capture (Hi-C) analysis revealed prominent contacts between telomeres and chromosomal arm regions containing replication origins proximal to binding sites for Taz1, a component of the Shelterin telomere protection complex. Strikingly, we find that Shelterin components are required for interactions between Taz1-associated chromosomal arm regions and telomeres. These analyses reveal an unexpected role for Shelterin components in genome reorganization in cells experiencing replication stress, with important implications for understanding the mechanisms governing replication and genome stability.

Shelterin | genome organization | replication | DNA damage | telomeres

The 3D organization of the eukaryotic genome creates specialized microenvironments that play important roles in various nuclear processes (1). In addition to regulation of gene expression, proper execution of the DNA replication program and DNA damage repair also involve dynamic organization of the genome (2, 3). Indeed, computational analyses indicate spatial segregation of replication origins based on their timing of firing during S-phase (4), suggesting that besides local chromatin structure, the 3D organization of chromosomes is an important contributing factor in the spatiotemporal control of replication (5, 6). Despite important advances, understanding the connections between diverse chromosomal events and genome organization remains an important challenge.

The complexities of genome organization have been studied in several model organisms, including the fission yeast *Schizosaccharomyces pombe*, for which the 3D organization has been explored at high resolution (7, 8). This simple eukaryote contains the basic chromosomal elements of more complex systems, including partitioning of the genome into euchromatin and heterochromatin domains. The *S. pombe* genome conforms to a Rabl organization pattern in which centromere clusters and telomere clusters are anchored at opposing sides of the nuclear periphery (9, 10). In addition, two key elements shape genome architecture: cohesin-dependent locally crumpled 50- to 100-kb repeating elements called "globules" on chromosome arms and the constraints imposed by the compaction of the chromatin fiber by heterochromatin domains such as at pericentromeric regions (8). The relatively small size of the *S. pombe* genome combined with the conserved genome organizational features provides an ideal system to explore connections between genome form and function.

Here, we show that cells carrying a mutation in the essential DNA-binding protein Sap1 display defects in replication progression, experience DNA damage, and undergo widespread genome reorganization. We find that several chromosomal arm regions associate specifically with telomeres in the *sap1* mutant. These interaction regions are generally adjacent to replication origins bound by Taz1 (11, 12), a counterpart of human TRF1/2 and a component of the Shelterin complex involved in telomeric end protection (13–15) and facilitation of proper replication of telomeres (16). Interestingly, Shelterin components are required to promote contacts between telomeres and chromosomal arm regions. We discuss the implications of these findings for understanding the mechanisms that ensure proper replication and protect genome stability.

Results

Defect in the Sap1 Protein Affects Genome Organization. Sap1 is an abundant nuclear protein that binds specific DNA elements distributed across the genome (17, 18). Multiple functions for Sap1 have been proposed, including a role in replication fork blocking (19–21), replication checkpoint activation (22), and genome organization (17). To gain further insight, we examined Sap1 subcellular localization. As previously shown (17), the Sap1 signal is concentrated within the nucleus in a diffuse pattern (Fig. S1*A*);

Significance

Genome organization affects many critical nuclear functions. Notably, the nuclear periphery has emerged as a specialized compartment for the regulation of transcription, replication, and DNA damage repair activities. Here, we find that cells carrying a mutation in the broadly distributed DNA-binding protein Sap1 experience replication stress and genome instability and undergo a genome reorganization featuring new contacts between chromosome arms and telomeres. These prominent new interactions are mediated by the Taz1–Shelterin telomere protection complex and include specific chromosome arm regions containing replication origins bound by Taz1. Our findings uncover an unexpected role for Shelterin in mediating genome reorganization in cells undergoing replication stress.

Author contributions: T.M. and S.I.S.G. designed research; T.M., N.T., E.M., and J.-M.B. performed the experiments; T.M., N.T., E.M., J.-M.B., P.F., J.D., and S.I.S.G. analyzed data; and T.M. and S.I.S.G. wrote the paper.

Reviewers: S.E.J., University of California, Los Angeles; and N.J.K., University of California, San Francisco.

The authors declare no conflict of interest.

Data deposition: The genome-wide datasets reported in this paper have been deposited in the Gene Expression Omnibus (GEO) repository, https://www.ncbi.nlm.nih.gov/geo (accession no. GSE96883).

[1]Present address: Department of Human Genetics, Yokohama City University Graduate School of Medicine, Yokohama 236-0004, Japan.

[2]To whom correspondence should be addressed. Email: grewals@mail.nih.gov.

This article contains supporting information online at www.pnas.org/lookup/suppl/doi:10.1073/pnas.1705527114/-/DCSupplemental.

however high-resolution microscopy revealed that Sap1 forms a matrix-like pattern (Fig. 1*A*). This localization was particularly interesting given the widespread distribution of Sap1 across the genome, including at solo LTRs and 13 copies of full-length *Tf2* retrotransposons (18), which are organized into nuclear foci (called "Tf bodies") in close proximity to the nuclear envelope (NE) (23, 24).

We considered that Sap1 binding to *Tf2* might be required for Tf body organization. To explore this possibility, we used a partial loss-of-function mutant, *sap1-1* (22). At restrictive temperature, *sap1-1* showed loss of Sap1 nuclear signal (Fig. S1*A*). Unlike the widely distributed WT Sap1 showing distinct peaks at nucleosome-free regions, the mutant protein was stable but unable to bind broadly across the genome (Fig. S1 *B*–*D*). ChIP analysis showed depletion of the mutant Sap1 from *Tf2* (Fig. 1*B* and Fig. S1*C*) correlating with an increase in *Tf2* foci in *sap1-1* cells (Fig. 1*C*), suggesting that Sap1 may have a role in clustering *Tf2* into Tf bodies.

Defects in Tf body organization in *sap1-1* cells might reflect broader changes in genome organization. We tested this possibility by performing FISH analysis of the *rtn1* locus, which was enriched for Sap1 binding in WT cells but was depleted in *sap1-1* cells (Fig. 1*B*). Compared with WT cells, the radial positioning of *rtn1* relative to the NE protein Bqt4 (25) was shifted more to the nuclear interior in *sap1-1* cells (Fig. 1*D*). Taken together, our results suggest that a defect in Sap1 affects genome organization, as indicated by disruption of Tf bodies and the altered positioning of other chromosome loci.

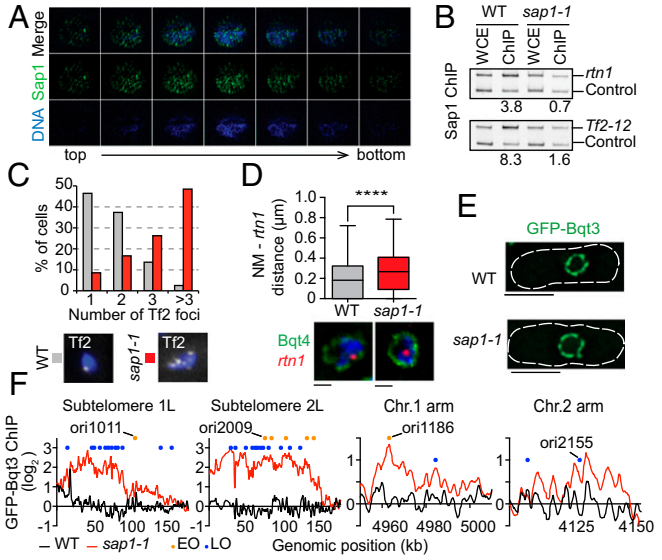

Fig. 1. Mutation in *sap1* affects the spatial positioning of chromosomes. (*A*) High-resolution microscopy analysis of Sap1 localization with DAPI staining. Images spanning from the top to the bottom of the cell are shown. (*B*) Sap1 ChIP-PCR analysis of *Tf2-12* and *rtn1* loci in WT and *sap1-1* cells. Relative ChIP enrichment is shown below. (*C*, *Upper*) FISH analysis of *Tf2* foci. The number of *Tf2* spots per cell was determined for WT and *sap1-1* cells. (*Lower*) Representative images are shown with DAPI staining. $n = 198$ for each strain. Images were collected using a 100 × 1.4 numerical aperture (NA) lens. (*D*, *Upper*) The position of the *rtn1* locus relative to the NE was determined by IF-FISH. (*Lower*) The box-plot diagram shows the distance distribution between the *rtn1* FISH signal and the NE (GFP-Bqt4). $^{****}P \leq 0.0001$ (three independent experiments, total $n = 457$ for WT and $n = 393$ for *sap1-1* cells; two-tailed Mann–Whitney test). (Scale bars, 0.5 μm.) (*E*) Focal plane images of WT and *sap1-1* cells expressing GFP-Bqt3. (Scale bars, 5 μm.) (*F*) GFP-Bqt3 ChIP enrichment across the subtelomeric region and several chromosomal arm regions in WT and *sap1-1* cells. Orange and blue circles represent early- and late-replication origins, respectively, as annotated by Hayashi and colleagues (48).

Nuclear Peripheral Association of Regions Containing Replication Origins in the *sap1* Mutant. Our results prompted us to perform a global analysis of genome positioning with respect to the nuclear periphery. To examine peripheral contacts, we performed ChIP-chip analysis of the nuclear membrane marker GFP-Bqt3 (25) and compared the contacts made with chromosome regions in WT and *sap1-1* cells. Importantly, GFP-Bqt3 decorated the NE in both WT and *sap1-1* cells (Fig. 1*E*). In agreement with the Rabl arrangement, specific regions of chromosomes associated with GFP-Bqt3. For example, GFP-Bqt3 was preferentially enriched at the centromere cores and telomeric regions of all three chromosomes (Fig. S2 *A* and *B*). In addition, we observed Bqt3 enrichment at *tRNA* clusters located at the heterochromatin boundaries of centromere 2 (Fig. S2*B*). Interestingly, GFP-Bqt3 remained associated with centromeres and telomeres in *sap1-1* cells and gained association with extended subtelomeric domains (>100 kb from each telomere) of chromosomes 1 and 2 but not chromosome 3 (Fig. 1*F* and Fig. S2*C*). Moreover, several regions of the chromosome arm showed GFP-Bqt3 enrichment in *sap1-1* cells, indicating a newly formed association with the nuclear periphery (Fig. 1*F* and Fig. S2*C*), whereas other regions, such as *tRNA* clusters, lost association with GFP-Bqt3 (Fig. S2*B*). These results demonstrate genome-wide changes in the contacts made with the NE in *sap1-1*.

Strikingly, we noticed that most regions that gained association with GFP-Bqt3 contained DNA replication origins (Table S1). The newly formed genomic contacts at extended subtelomeric domains coincided with late origin cluster zones (Fig. 1*F* and Fig. S2*C*) (11). The specific association of selected chromosome regions containing origins with the nuclear periphery in *sap1-1* cells suggested a possible connection between DNA replication activity and genome reorganization.

The *sap1* Mutant Shows DNA Replication Defects. We next examined if *sap1-1* affects DNA replication. To do so, we used the *cdc10-v50* mutant to synchronize cells and monitor DNA replication progression from G1 arrest. FACS analysis revealed that *sap1-1* cells spent a comparatively longer time in S-phase than WT cells (Fig. 2*A*), suggesting possible defects in replication in the mutant cells. To test for such defects, we examined the genome-wide replication profile by measuring BrdU incorporation in WT and *sap1-1* cells released from G1 arrest in the presence of hydroxyurea (HU). As expected, efficient firing of replication origins occurred in WT cells (Fig. S3*A*). However, BrdU incorporation in *sap1-1* cells was inefficient, particularly at subtelomeric regions containing clusters of late-replication origins that showed replication in this experimental set-up involving *cdc10-v50* (Fig. 2*B* and Fig. S3*B*). Some chromosomal arm regions that showed association with GFP-Bqt3 in *sap1-1* cells also showed low BrdU enrichment (Fig. 2*B*).

To investigate the effect of *sap1-1* on replication further, we examined its impact on the genome-wide distribution of Mcm6 protein during S-phase. Mcm6 is a component of the MCM (mini chromosome maintenance) complex, which is a putative DNA replicative helicase required for replication initiation and elongation (26). We found a striking reduction of Mcm6 in *sap1-1* cells, particularly between replication origins, as is consistent with abnormal replication progression (Fig. 2*C* and Fig. S3 *C* and *D*). Thus, global replication defects are indeed associated with loss of Sap1 function; however, the exact mechanism remains unknown.

***sap1* Mutant Cells Accumulate ssDNA and DNA Damage-Repair Foci.** Cells that experience replication stress tend to accumulate ssDNA, which can lead to genome instability (27, 28). To detect ssDNA, we quantified the number of Rad11 foci. Rad11 is a component of an ssDNA-binding complex called "replication protein A" (RPA), which is involved in DNA replication and/or DNA damage repair (28). Generally, WT S-phase cells have multiple faint Rad11 signals, and some mononucleated cells form a discrete single Rad11 focus in the nucleolus. However, we observed a significantly higher

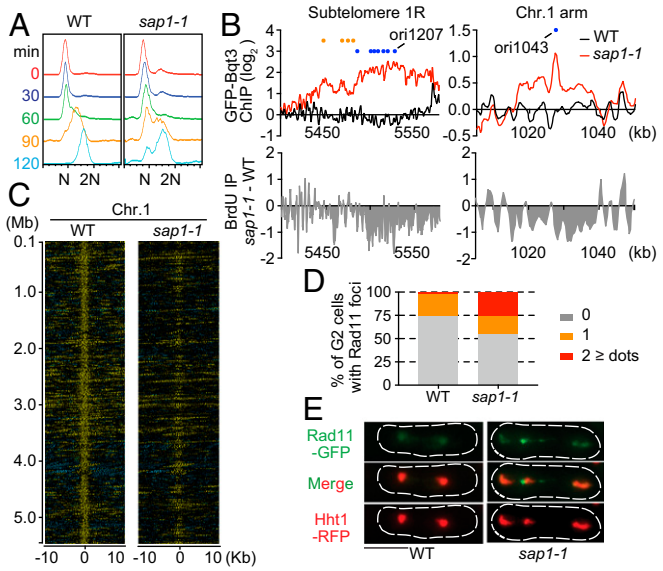

Fig. 2. *sap1-1* impacts DNA replication. (*A*) FACS profile of DNA content in WT and *sap1-1* cells. Cells carrying the *cdc10-v50* mutation were arrested in G1 and then released. Numbers on the left indicate the time in minutes after the release. (*B*) DNA replication profile in WT and *sap1-1* cells. The differences in BrdU incorporation were plotted across subtelomeric domains and at certain chromosome arm regions that gained association with Bqt3 in *sap1-1* cells. GFP-Bqt3 ChIP enrichment in WT and *sap1-1* is shown on the top. Orange and blue circles represent early- and late-replication origins, respectively. (*C*) Heat maps of Chr.1 for both WT and *sap1-1* cells showing the Mcm6 ChIP signal around replication origins (10-kb regions). (*D*) Rad11-GFP forms discrete foci in *sap1-1* cells. Cells expressing Rad11-GFP (green) and Hht1(histone H3)-RFP (red) were grown at 33 °C for 6 h. The percentage of mononuclear cells with Rad11-GFP foci ($n = 84$ for WT and $n = 103$ for *sap1-1* cells) is shown. (*E*) Mitotic cells expressing Rad11-GFP (green) and Hht1-RFP (red). *sap1-1* cells enter mitotic nuclear division in the presence of Rad11 foci. Chromatin (Hht1-RFP) appears fragmented and lags during the M-phase in *sap1-1* cells. Rad11-GFP forms a fine bridge between the daughter nuclei and is enriched near fragmented chromatin masses. (Scale bar, 5 μm.)

number of *sap1-1* cells than WT cells displaying two or more Rad11 foci in the chromatin hemisphere (Fig. 2*D* and Fig. S4*A*). Moreover, time-lapse microscopy revealed that *sap1-1* cells with Rad11 foci enter mitosis, resulting in the fragmentation of chromosomes (Fig. 2*E*, Fig. S4*B*, and Movies S1 and S2). This result indicates that replication stress may be a potential source of genome instability in *sap1-1* cells.

We also examined DNA damage-repair foci formation by monitoring the homologous recombination (HR) factor Rad52. Consistent with previous work (22), ~55% of *sap1-1* cells contained one or more Rad52 foci, whereas 11% of WT cells contained a single Rad52 focus (Fig. S4*C*). Furthermore, *sap1-1 rad52Δ* double-mutant cells showed a synthetic growth defect (Fig. S4*D*). Taken together, our study and others suggest that cells carrying a mutation in Sap1 experience problems with replication progression, ultimately resulting in the accumulation of DNA damage (22).

The *sap1-1* Genome Contains Rearrangements. Replication defects and DNA damage in *sap1-1* cells could cause genome instability, such as chromosomal rearrangements. Interestingly, *sap1-1* cells frequently produced revertants capable of growing at an otherwise nonpermissive temperature (37 °C) (Fig. 3*A*). Microarray comparative genome hybridization (CGH) analysis of a revertant showed amplification of the region encompassing the *sap1-1* locus (Fig. 3*B* and Fig. S5*A*). We confirmed the duplication of this region, which resulted in a slight increase in Sap1 mutant protein (Fig. S5*B*). The boundaries of the amplified region contain *wtf* (repeats often associated with *Tf LTRs*) bound by Sap1 in WT cells (Fig. 3*B*). Junction PCR analysis and subsequent Sanger sequencing revealed that the copy number gain resulted from direct tandem-oriented duplication (Fig. 3*C* and Fig. S5 *C* and *D*).

This rearrangement likely confers a survival advantage from the amplification of the *sap1-1* region and suppression of the mutant phenotype. However, we found a more widespread destabilizing effect that involved other repeat structures, including *wtfs* in other parts of the *sap1-1* genome. In addition to *wtfs* that flank *sap1*, recombination occurred between other tandem copies of *wtfs* (such as *wtf18–wtf13*) in *sap1-1* cells cultured at a semipermissive temperature (33 °C) (Fig. 3*C*). We also detected rearrangements in the subtelomeric repeats (Fig. S5*E*). These results clearly show that *sap1-1* is prone to more widespread genome instability.

Because substrates for recombination can be generated by stalled or collapsed replication forks (29), we looked for replication defects at *wtf* elements. Indeed, 2D gel analysis revealed prominent replication fork pausing at the *wtf9* region in *sap1-1* cells (Fig. 3*D*). We also found that Rad52 was required for tandem duplication mediated by *wtf* repeats (Fig. S5*F*). Strikingly, *sap1-1* cells lacking the well-defined checkpoint effector kinases Chk1 or Cds1 showed increased rearrangements (Fig. 3 *A* and *E*), suggesting that components of DNA damage and replication checkpoints are critical for suppressing genome instability in *sap1-1* cells.

We also tested whether de-repression of *wtf* elements could be involved in promoting rearrangement. The histone deacetylases Clr3 and Clr6 have been implicated in the repression of *wtf* (30). However, defects in the histone deacetylases had no effect on *wtf*-mediated genomic rearrangements (Fig. S5*G*). Therefore, de-repression of *wtf* alone is not sufficient to trigger rearrangements. Rather, genome instability in *sap1-1* is linked to defective replication

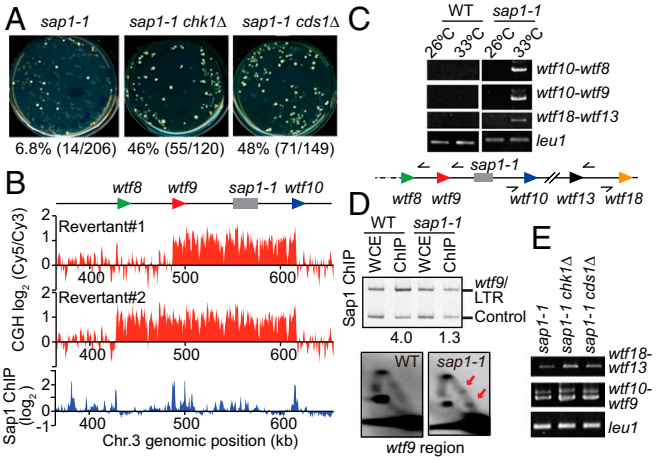

Fig. 3. Sap1 promotes genome integrity. (*A*) Frequency of revertant generation in *sap1-1* cells. The percentage of revertants (number of revertants/total number of colonies) is shown below. (*B*) Array CGH analysis of two independent revertants. The $\log_2$ (cy5/cy3 signal ratio) is shown across copy number gain regions in chromosome 3. Relative genomic positions of the *sap1* gene and *wtf* elements are shown on the top (not to exact scale). ChIP-chip of Sap1 is shown below. (*C*) Junction PCR to detect *wtf*-mediated duplication. The *sap1-1* strain was successively cultured at a semipermissive temperature (33 °C) in liquid medium. *leu1* was used as a PCR control. Arrowheads indicate divergently oriented primers used for junction PCR. (*D*) Sap1 ChIP-PCR (*Upper*) and 2D gel analysis (*Lower*) of the *wtf9* region. Relative ChIP enrichment is shown below the panel. Arrows in 2D gel analysis indicate fork pausing signals. (*E*) Junction PCR analysis of the indicated mutant strains. *leu1* was used as a PCR control.

and DNA damage repair and is also accompanied by alterations in 3D genome organization.

Genome-Wide Chromosome Conformation Capture Analysis Reveals Specific Interactions in the *sap1* Mutant. To obtain a detailed view of genome contacts in *sap1-1*, we performed genome-wide chromosome conformation capture (Hi-C) analyses. Two biological replicates were generated for both WT and *sap1-1* cells. The Hi-C contact maps were highly reproducible. We found that previously described features of genome organization such as centromere and telomere clusters and heterochromatin-mediated intra- and interchromosomal arm interactions observed within centromere proximal regions were unaffected in *sap1-1* cells (Fig. 4*A* and Fig. S6*A*). Scaling analysis revealed a slow decay in contact probability at distances <100 kb followed by a faster decay in *sap1-1* cells, as in WT cells (Fig. S6*B*), indicating the existence of globules. Indeed, cohesin-dependent globules along chromosome arms were evident in *sap1-1* cells, and the depletion of contact frequency (insulation) between regions separated by cohesin-bound globule boundaries was not affected (Fig. S6*C*). Consistently, the binding profile of cohesin subunit Psc3 was unchanged in *sap1-1* cells (Fig. S6*D*).

Strikingly, our analyses revealed several prominent new contacts in the *sap1-1* mutant that were not visible in WT cells. These contacts could be detected in *sap1-1* cells cultured at semipermissive temperature for only 6 h. A common feature among all new contacts was the involvement of telomeric regions of chromosomes 1 and 2 (Fig. 4*B*). We observed newly formed contacts between the subtelomeric regions of the two short arms (*tel1R* and *tel2L*) and all three centromeres (Fig. 4*B*). Intriguingly, we also observed prominent interactions between telomeres and specific arm regions (Fig. 4*B*). These interactions were mainly restricted to the arms of chromosomes 1 and 2 and were not observed on chromosome 3 (Fig. S6*E*).

We further validated the new contacts using live-cell microscopy and chromosome conformation capture (3C) assays. Time-lapse

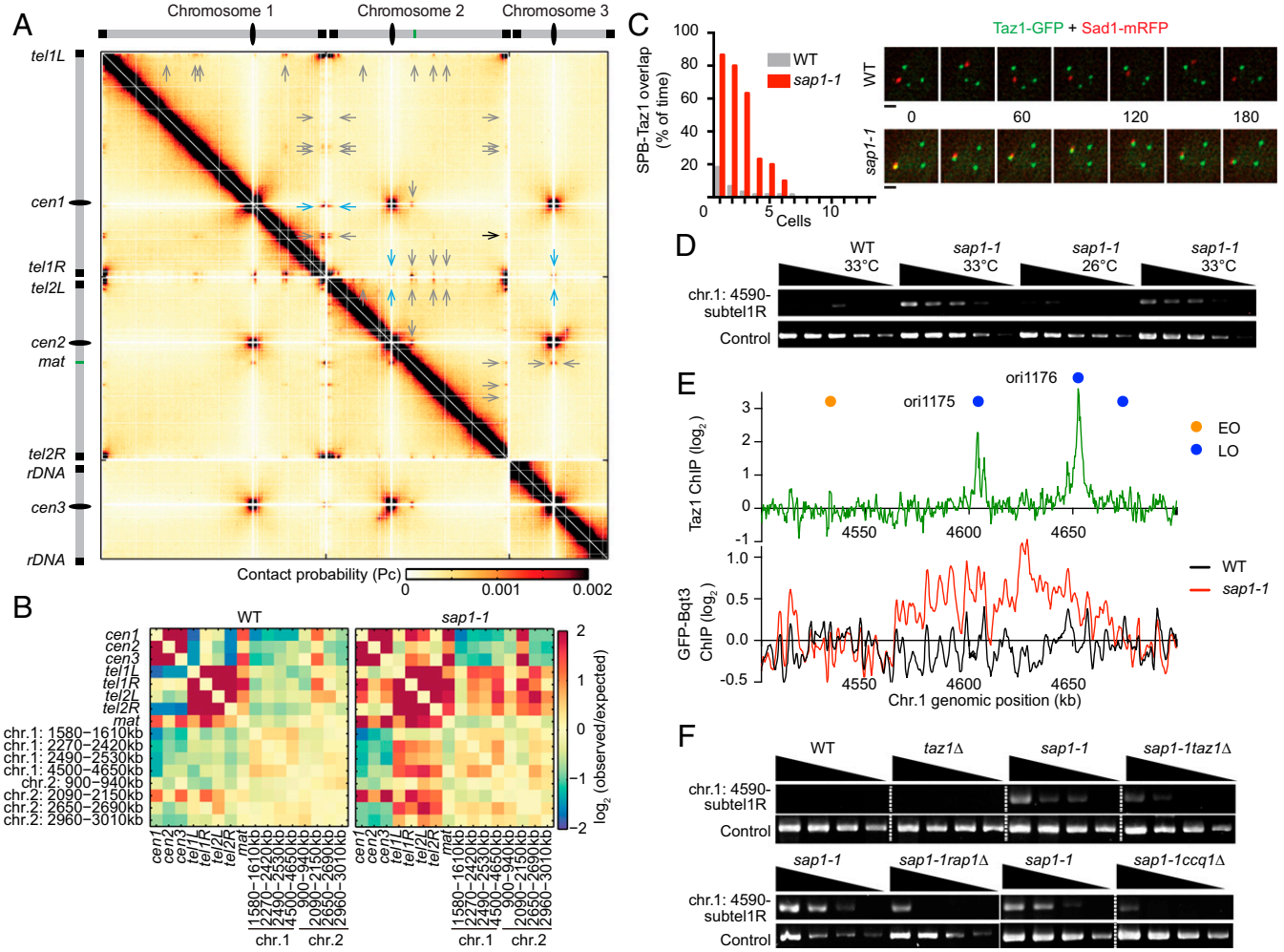

Fig. 4. Hi-C reveals new specific interactions in *sap1-1* mutants. (*A*) Genome-wide Hi-C heatmap for *sap1-1* at 10-kb resolution. Gray and blue arrows indicate the arm–subtelomere and centromere–subtelomere interactions, respectively. (*B*) Log_2 (observed/expected) contact frequency between centromeres, telomeres, and loci with emergent interactions in *sap1-1* for WT (*Left*) and *sap1-1* (*Right*) cells. (*C*) Time-lapse observation of Taz1-GFP (green) and Sad1-mRFP (red). (*Left*) The percentage of time points showing colocalization of Taz1-GFP and Sad1-mRFP during the 10-min time lapse at 10-s intervals. Thirteen WT and *sap1-1* cells were scored. (*Right*) Representative time-lapse images. Numbers indicate the time in seconds. (Scale bars, 1 μm). (*D*) 3C PCR analysis of *sap1-1*–specific interactions (chr.1: 4,590-kb region and subtelomere 1R, ∼1 Mb apart). A close-range interaction (≤10 kb) was used as a 3C control. Twofold serial dilutions of the 3C library were used as a PCR template. Strains were initially cultured at 26 °C and then were shifted to 33 °C for 6 h. (*E*) ChIP-chip of Taz1 and GFP-Bqt3 is shown at chromosome arms where new interactions emerge in *sap1-1* cells (chr.1: 4,590-kb region and subtelomere 1R). Orange and blue circles represent the early- and late-replication origins, respectively. (*F*) 3C PCR analysis of the *sap1-1*–specific interaction (chr.1: 4,590-kb region and subtelomere 1R) in the indicated mutants. Strains were initially cultured at 26 °C and then were shifted to 33 °C for 6 h. A close-range interaction (≤10 kb) was used as a 3C control. Twofold serial dilutions of the 3C library were used as a PCR template.

microscopy revealed an association between centromeres and telomeres in a significant proportion of *sap1-1* cells (Fig. 4*C* and Movies S3 and S4), in contrast to WT cells (Movies S5 and S6). Moreover, our 3C experiment detected an interaction between a region on the chromosome 1 arm (the genomic position of the 4,500- to 4,650-kb region) and *tel1R* in *sap1-1* cells, which are ∼1 Mb apart in linear genomic distance (Fig. 4*D*). This interaction was specific to *sap1-1* cells and was detected only when cells were cultured at semipermissive temperature.

To exclude the possibility that our 3C experiments detected genomic rearrangements rather than new interactions, we performed PCR analysis using genomic DNA from *sap1-1* cells. Importantly, no PCR amplification could be observed (Fig. S6*F*). Based on these results, we conclude that *sap1-1* mutant cells, which show replication defects and genome instability, undergo genome reorganization resulting in specific new interactions with telomeres.

Shelterin Mediates New Interactions. We noted that many of the arm regions that contacted telomeres contained previously described late origins that are bound by Taz1 (Fig. S6*E*) (11, 12). Notably, Taz1 peaks were generally observed at the edges rather than at the center of these interacting regions. This observation may be a consequence of our Hi-C analyses that excluded Taz1-bound repetitive telomeric sequences, which might interact directly with chromosomal internal sites showing Taz1 peaks. Thus, the detected interactions most likely reflect contacts between distal sequences neighboring direct interaction sites (i.e., telomeres and Taz1-associated arm regions).

We investigated whether Taz1–Shelterin affects interactions between telomeres and arm regions. To do so, we performed 3C analyses in *sap1-1* cells lacking Taz1 or other Shelterin subunits such as Rap1 or Ccq1. Remarkably, the loss of any of these factors significantly reduced the interaction between *tel1R* and a Taz1-associated arm region (chromosome 1: 4,500- to 4,650-kb region) that contains late origins and associates with the nuclear periphery in *sap1-1* cells (Fig. 4 *E* and *F*). Taz1 and Rap1 also interact with Bqt1 and Bqt2, which connect telomeres to the spindle pole body (SPB) upon entry into meiosis (31). However, telomeric association of arm regions was not affected in *sap1-1 bqt1Δ* and *sap1-1 bqt2Δ* double mutants (Fig. S6*G*). Together, these results implicate Taz1–Shelterin in mediating new interactions between chromosome arm regions and telomeres in *sap1-1* cells.

We also examined whether Shelterin components affects centromere–telomere contacts in *sap1-1* cells. We found that in *sap1-1* cells lacking Rap1, centromeres and telomeres remained associated with the nuclear periphery (Fig. S7 *A* and *B*); however, the number of cells showing association between these loci decreased (Fig. S7*C*). Thus, in addition to facilitating connections between telomeres and chromosome arm regions, Shelterin components also seems necessary to mediate centromere–telomere contacts in *sap1-1*.

We wondered whether the genome reorganization observed in *sap1-1* cells in response to replication stress is biologically relevant. Because certain types of DNA damage are targeted to nuclear compartments for specialized repair (32), we speculated that Shelterin-mediated association of arm regions with telomeres might affect the DNA damage-repair process. Indeed, the loss of Ccq1 or Rap1 in *sap1-1* mutant cells resulted in a considerable increase in the number of Rad52 repair foci (Fig. S7*D*).

Discussion

The organization of eukaryotic genomes impacts many aspects of genome function, including replication and DNA-repair processes (2, 3). We find that cells carrying a mutation in Sap1 that show replication defects and genome instability undergo changes in genome organization. A remarkable finding is that components of the Shelterin telomere protection complex promote interactions between telomeres and specific chromosomal arm regions. These results suggest an additional role for Shelterin in promoting genome reorganization with implications for understanding mechanisms that protect genome stability.

Sap1 has been suggested to play an important role in replication fork pausing at *rDNA* and retrotransposon *LTRs* (18, 20, 21). We show that Sap1 also facilitates replication progression, as indicated by 2D gel, Mcm6 localization, and BrdU incorporation analyses. In addition, replication defects are suggested by the accumulation of ssDNA and DNA repair foci in *sap1-1* cells. Sap1 might impact replication through local chromatin changes, e.g., by affecting nucleosome occupancy (33). Another possibility is that Sap1, with its matrix-like nuclear localization, might serve as an architectural protein that binds and constrains chromosomes to promote their spatial positioning and proper replication. Such a role might be analogous to DNA-binding proteins in higher eukaryotes, such as CTCF, which recruits cohesin involved in genome organization (34). However, Sap1 is dispensable for cohesin-dependent globules. Instead, our preliminary analysis indicates that Sap1 copurifies with topoisomerase II (https://ccrod.cancer.gov/confluence/download/attachments/101483286/Sap1TopII.pdf?api=v2) implicated in replication and chromosome organization (35, 36). Regardless of its exact function, loss of Sap1 function affects proper replication, structural integrity, and organization of the genome.

sap1-1 cells show widespread genome reorganization, including association of arm regions with telomeres and the nuclear periphery. Because the affected arm regions contain replication origins and experience replication stress, it is conceivable that Sap1 indirectly affects genome organization through its impact on DNA replication/repair. Moreover, a low level of genomic rearrangements might contribute to the new interactions detected. To this end, we note that specific new interactions occur rapidly in cells that are cultured at a semipermissive temperature for only 6 h. Although these interactions potentially could lead to recombination events, whole-genome sequencing of *sap1-1* did not reveal translocations between the newly interacting loci.

Our finding that Taz1–Shelterin mediates interactions between telomeres and arm regions has implications for understanding replication control and genome stability. Late firing of Taz1-affected origins requires telomere-associated Rif1, which also has been implicated in DNA repair (37, 38). However, Rif1 binds only a subset of Taz1-associated late origins (11, 38, 39), and it is conceivable that Shelterin-mediated telomeric association of these origins allows Rif1 acquisition to promote proper replication and DNA repair. In other words, Taz1-bound late origins in telomeric and arm regions might be controlled in a shared nuclear compartment. The physical proximity of regions experiencing replication stress to Rif1-enriched telomeres may also facilitate the resolution of DNA entanglements (40) and promote chromosome healing, in which telomerase "heals" dsDNA breaks (41). Finally, localization of these regions to the nuclear peripheral compartment may provide an opportunity to suppress and repair DNA damage, as observed in other systems (32, 42, 43). In this regard, we find that disruption of the telomeric association of arm regions in *sap1-1* cells lacking Shelterin components correlates with increased accumulation of DNA damage. Moreover, certain Shelterin components show negative genetic interactions with DNA repair and checkpoint factors (44).

Collectively, these results link changes in genome organization to replication stress, which is an early driver of oncogenesis (45). Tandem duplication of chromosomal segments is a dominant class of structural change found in breast and ovarian cancers (46) and is thought to arise from the repair of replication stress-associated DNA breaks (47). Insights gained from *S. pombe* may aid studies in higher eukaryotes, particularly those focusing on the mechanisms underlying structural abnormalities and nuclear reorganization in replication-stressed cells.

Materials and Methods

WT and mutant strains were initially cultured in yeast extract adenine (YEA)-rich medium at 26 °C and then were shifted to 33 °C for 6 h, unless otherwise

indicated. Growth conditions used to detect rearrangements, BrdU incorporation, and 2D gel analysis in *sap1-1* cells are detailed in *SI Materials and Methods*. A description of Hi-C, 3C, ChIP-chip, BrdU incorporation, nucleosome mapping, CGH, Junction PCR, Southern blotting, 2D gel analysis, and FISH procedures can be found in *SI Materials and Methods*. Primers used in this study are listed in Table S2.

ACKNOWLEDGMENTS. We thank E. Noguchi, Y. Hiraoka, and J. P. Cooper for strains, B. Arcangioli for anti-Sap1 antibody, H. Masukata for strains and anti-Mcm6 antibody; G. Fudenberg, L. Mirny, H. Diego Folco, and S. Mehta for helpful contributions; J. Barrowman for help in preparing and editing the manuscript; and members of the S.I.S.G. laboratory for helpful suggestions. This work was supported by the Intramural Research Program of the National Institutes of Health, National Cancer Institute.

1. Misteli T (2007) Beyond the sequence: Cellular organization of genome function. *Cell* 128:787–800.
2. Aparicio OM (2013) Location, location, location: It's all in the timing for replication origins. *Genes Dev* 27:117–128.
3. Seeber A, Gasser SM (2016) Chromatin organization and dynamics in double-strand break repair. *Curr Opin Genet Dev* 43:9–16.
4. Pichugina T, et al. (2016) A diffusion model for the coordination of DNA replication in *Schizosaccharomyces pombe*. *Sci Rep* 6:18757.
5. Aladjem MI, Redon CE (2017) Order from clutter: Selective interactions at mammalian replication origins. *Nat Rev Genet* 18:101–116.
6. Rhind N, Gilbert DM (2013) DNA replication timing. *Cold Spring Harb Perspect Biol* 5: a010132.
7. Kim KD, Tanizawa H, Iwasaki O, Noma K (2016) Transcription factors mediate condensin recruitment and global chromosomal organization in fission yeast. *Nat Genet* 48:1242–1252.
8. Mizuguchi T, et al. (2014) Cohesin-dependent globules and heterochromatin shape 3D genome architecture in *S. pombe*. *Nature* 516:432–435.
9. Funabiki H, Hagan I, Uzawa S, Yanagida M (1993) Cell cycle-dependent specific positioning and clustering of centromeres and telomeres in fission yeast. *J Cell Biol* 121: 961–976.
10. Mizuguchi T, Barrowman J, Grewal SI (2015) Chromosome domain architecture and dynamic organization of the fission yeast genome. *FEBS Lett* 589:2975–2986.
11. Tazumi A, et al. (2012) Telomere-binding protein Taz1 controls global replication timing through its localization near late replication origins in fission yeast. *Genes Dev* 26:2050–2062.
12. Zofall M, Smith DR, Mizuguchi T, Dhakshnamoorthy J, Grewal SIS (2016) Taz1-Shelterin promotes facultative heterochromatin assembly at chromosome-internal sites containing late replication origins. *Mol Cell* 62:862–874.
13. de Lange T (2005) Shelterin: The protein complex that shapes and safeguards human telomeres. *Genes Dev* 19:2100–2110.
14. Ferreira MG, Cooper JP (2001) The fission yeast Taz1 protein protects chromosomes from Ku-dependent end-to-end fusions. *Mol Cell* 7:55–63.
15. Miyoshi T, Kanoh J, Saito M, Ishikawa F (2008) Fission yeast Pot1-Tpp1 protects telomeres and regulates telomere length. *Science* 320:1341–1344.
16. Miller KM, Rog O, Cooper JP (2006) Semi-conservative DNA replication through telomeres requires Taz1. *Nature* 440:824–828.
17. de Lahondès R, Ribes V, Arcangioli B (2003) Fission yeast Sap1 protein is essential for chromosome stability. *Eukaryot Cell* 2:910–921.
18. Zaratiegui M, et al. (2011) CENP-B preserves genome integrity at replication forks paused by retrotransposon LTR. *Nature* 469:112–115.
19. Jacobs JZ, et al. (2015) Arrested replication forks guide retrotransposon integration. *Science* 349:1549–1553.
20. Krings G, Bastia D (2005) Sap1p binds to Ter1 at the ribosomal DNA of *Schizosaccharomyces pombe* and causes polar replication fork arrest. *J Biol Chem* 280: 39135–39142.
21. Mejía-Ramírez E, Sánchez-Gorostiaga A, Krimer DB, Schvartzman JB, Hernández P (2005) The mating type switch-activating protein Sap1 Is required for replication fork arrest at the rRNA genes of fission yeast. *Mol Cell Biol* 25:8755–8761.
22. Noguchi C, Noguchi E (2007) Sap1 promotes the association of the replication fork protection complex with chromatin and is involved in the replication checkpoint in *Schizosaccharomyces pombe*. *Genetics* 175:553–566.
23. Cam HP, Noma K, Ebina H, Levin HL, Grewal SI (2008) Host genome surveillance for retrotransposons by transposon-derived proteins. *Nature* 451:431–436.
24. Tanaka A, et al. (2012) Epigenetic regulation of condensin-mediated genome organization during the cell cycle and upon DNA damage through histone H3 lysine 56 acetylation. *Mol Cell* 48:532–546.
25. Chikashige Y, et al. (2009) Membrane proteins Bqt3 and -4 anchor telomeres to the nuclear envelope to ensure chromosomal bouquet formation. *J Cell Biol* 187:413–427.
26. Forsburg SL (2004) Eukaryotic MCM proteins: Beyond replication initiation. *Microbiol Mol Biol Rev* 68:109–131.
27. Lambert S, Carr AM (2013) Impediments to replication fork movement: Stabilisation, reactivation and genome instability. *Chromosoma* 122:33–45.
28. Sabatinos SA, Forsburg SL (2015) Managing single-stranded DNA during replication stress in fission yeast. *Biomolecules* 5:2123–2139.
29. Lambert S, Watson A, Sheedy DM, Martin B, Carr AM (2005) Gross chromosomal rearrangements and elevated recombination at an inducible site-specific replication fork barrier. *Cell* 121:689–702.
30. Nicolas E, et al. (2007) Distinct roles of HDAC complexes in promoter silencing, antisense suppression and DNA damage protection. *Nat Struct Mol Biol* 14:372–380.
31. Chikashige Y, et al. (2006) Meiotic proteins bqt1 and bqt2 tether telomeres to form the bouquet arrangement of chromosomes. *Cell* 125:59–69.
32. Nagai S, et al. (2008) Functional targeting of DNA damage to a nuclear pore-associated SUMO-dependent ubiquitin ligase. *Science* 322:597–602.
33. Tsankov A, Yanagisawa Y, Rhind N, Regev A, Rando OJ (2011) Evolutionary divergence of intrinsic and trans-regulated nucleosome positioning sequences reveals plastic rules for chromatin organization. *Genome Res* 21:1851–1862.
34. Ong CT, Corces VG (2014) CTCF: An architectural protein bridging genome topology and function. *Nat Rev Genet* 15:234–246.
35. Branzei D, Foiani M (2010) Maintaining genome stability at the replication fork. *Nat Rev Mol Cell Biol* 11:208–219.
36. Uemura T, et al. (1987) DNA topoisomerase II is required for condensation and separation of mitotic chromosomes in *S. pombe*. *Cell* 50:917–925.
37. Zimmermann M, Lottersberger F, Buonomo SB, Sfeir A, de Lange T (2013) 53BP1 regulates DSB repair using Rif1 to control 5′ end resection. *Science* 339: 700–704.
38. Hayano M, et al. (2012) Rif1 is a global regulator of timing of replication origin firing in fission yeast. *Genes Dev* 26:137–150.
39. Kanoh Y, et al. (2015) Rif1 binds to G quadruplexes and suppresses replication over long distances. *Nat Struct Mol Biol* 22:889–897.
40. Zaaijer S, Shaikh N, Nageshan RK, Cooper JP (2016) Rif1 regulates the fate of DNA entanglements during mitosis. *Cell Reports* 16:148–160.
41. Pennaneach V, Putnam CD, Kolodner RD (2006) Chromosome healing by de novo telomere addition in Saccharomyces cerevisiae. *Mol Microbiol* 59:1357–1368.
42. Oza P, Jaspersen SL, Miele A, Dekker J, Peterson CL (2009) Mechanisms that regulate localization of a DNA double-strand break to the nuclear periphery. *Genes Dev* 23: 912–927.
43. Schober H, Ferreira H, Kalck V, Gehlen LR, Gasser SM (2009) Yeast telomerase and the SUN domain protein Mps3 anchor telomeres and repress subtelomeric recombination. *Genes Dev* 23:928–938.
44. Ryan CJ, et al. (2012) Hierarchical modularity and the evolution of genetic interactomes across species. *Mol Cell* 46:691–704.
45. Halazonetis TD, Gorgoulis VG, Bartek J (2008) An oncogene-induced DNA damage model for cancer development. *Science* 319:1352–1355.
46. McBride DJ, et al. (2012) Tandem duplication of chromosomal segments is common in ovarian and breast cancer genomes. *J Pathol* 227:446–455.
47. Costantino L, et al. (2014) Break-induced replication repair of damaged forks induces genomic duplications in human cells. *Science* 343:88–91.
48. Hayashi M, et al. (2007) Genome-wide localization of pre-RC sites and identification of replication origins in fission yeast. *EMBO J* 26:1327–1339.
49. Imakaev M, et al. (2012) Iterative correction of Hi-C data reveals hallmarks of chromosome organization. *Nat Methods* 9:999–1003.
50. Cam HP, et al. (2005) Comprehensive analysis of heterochromatin- and RNAi-mediated epigenetic control of the fission yeast genome. *Nat Genet* 37:809–819.
51. Chikashige Y, et al. (1989) Composite motifs and repeat symmetry in *S. pombe* centromeres: Direct analysis by integration of NotI restriction sites. *Cell* 57:739–751.
52. Yamane K, et al. (2011) Asf1/HIRA facilitate global histone deacetylation and associate with HP1 to promote nucleosome occupancy at heterochromatic loci. *Mol Cell* 41:56–66.

Supporting Information

Mizuguchi et al. 10.1073/pnas.1705527114

SI Materials and Methods

Hi-C and 3C Analysis. The 3C and Hi-C libraries were generated as previously described using the restriction enzyme HindIII (8). 3C PCR was performed using the primers listed in Table S2. Hi-C data were mapped, and reads were filtered as described (8). Corrected contact probability matrices at 10-kb resolution were obtained using iterative correction (49). Both steps were performed using the hiclib library for python, publicly available at https://bitbucket.org/mirnylab/hiclib. Corrected Hi-C contact maps (Fig. 4*A* and Fig. S6*A*) and the rate of decay of intra-arm Pc values and the insulation plot (Fig. S6 *B* and *C*) were created as previously described (8).

ChIP and ChIP-ChIP. ChIP was performed as previously described using anti-Sap1 antibody (rabbit polyclonal, a gift from B. Arcangioli, Dynamics of the Genome Unit, Department of Genomes and Genetics, Institut Pasteur, Paris), anti-Mcm6 (rabbit polyclonal, a gift from H. Masukata, Department of Biological Sciences, Graduate School of Science, Osaka University, Osaka), or anti-GFP (ab290; Abcam) for GFP-Bqt3 (50). Immunoprecipitated and input DNA were analyzed by quantitative duplex PCR using the primers listed in Table S2. Relative ChIP enrichment was determined as the ratio of the intensity of the duplex PCR product of the target to the control locus from ChIP samples normalized to an input DNA. Labeling, hybridization, and analysis of the microarray experiments were performed as described in ref. 12 using the genome-wide tiling microarray platform (50).

Mcm6 ChIP Plot. HU was used to arrest WT and *sap1-1* cells at S-phase. The $\log_2$ ratio of Mcm6 ChIP enrichment in WT cells revealed distinct regions of enrichment across the genome. The Mcm6 signal was particularly enhanced at the subtelomeric regions and appeared as distinct peaks distributed across the genome. The 332 most prominent (nontelomeric) peaks on chromosome 1 were selected for specific comparison of Mcm6 binding in WT and *sap1-1* cells. The heat map in Fig. 2*C* was generated using Java TreeView and shows the $\log_2$ ratio (ChIP/INPUT) 10 kb on either side of the 332 identified peaks in WT and *sap1-1* cells.

BrdU Incorporation. DNA replication profiles were obtained by measuring the BrdU incorporation as previously described (12). The *cdc10-v50* strains carrying the herpes simplex virus thymidine kinase expression module *Pnmt1-TK* and the human nucleoside transporter module *Padh1-hENT* were grown at 35 °C for 4 h and were released from the G1 block by transfer to medium supplemented with 200 μM BrdU and 10 mM HU at 26 °C for 90 min. BrdU-labeled DNA was extracted and used for immunoprecipitation with mouse anti-BrdU antibody (BD Pharmingen). Labeling, hybridization, and analysis of the microarray experiments were performed as for ChIP-chip experiments.

Immunofluorescence and FISH. Immunofluorescence and FISH experiments were carried out as described (9, 23). Anti-Sap1 antibody (rabbit polyclonal, a gift from B. Arcangioli) and anti-GFP (ab290; Abcam) were used for immunofluorescence. The probe used for FISH analysis was prepared using *TF2*-ORF plasmid and pRS140 (centromeric repeat DNA) (23, 51). A position-specific probe for *rtn1* was generated by long-range PCR using the primers listed in Table S2. Optical section data were collected using a DeltaVision Elite microscope (GE Healthcare) and were subsequently deconvolved using SoftWoRX 6.0 (GE Healthcare).

Live-Cell Imaging. For time-lapse images, cells were mounted in a glass-bottomed culture dish coated with lectin and were imaged on a DeltaVision Elite microscope (GE Healthcare) with a 100× 1.4 NA Plan Super Apochromat oil lens (Olympus). Thirteen 0.3-μm *z*-sections were acquired at each time point and subsequently were deconvolved using SoftWoRX 6.0 (GE Healthcare). Further image processing, including maximum intensity projections and time-lapse observation, was performed using SoftWoRX 6.0 (National Institutes of Health). A focal plane of unprocessed image and projection image was analyzed to determine colocalization of telomeres (Taz1-GFP) and SPBs (Sad1-mRFP).

Plate Assay for *sap1-1* Revertant Isolation. WT and mutant cells cultured at 26 °C were spread onto rich YEA agar plates and allowed to grow for 5 d. After colony formation, cells were replica plated and incubated at 37 °C for 7 d. Revertant colonies were counted and isolated for subsequent experiments.

Liquid Culture for *sap1-1* Revertant Isolation. Mutant strains were initially cultured at 26 °C. Rearrangements of *wtf* elements were detected in cells that were inoculated at a cell density of OD_{600} ~0.02, shifted to 33 °C, and incubated for 3 d with periodic dilution to maintain a cell density of OD_{600} 0.02–1.2. Isolated genomic DNA was used for junction PCR experiments to detect *wtf*-mediated tandem duplication.

Junction PCR and Mapping the Recombination Junction. Genomic rearrangements mediated by *wtf* elements were detected by PCR using Takara Ex Taq HS (Takara Bio). The primers are listed in Table S2. PCR conditions used with *wtf10–wtf8* and *wtf10–wtf9* primer pairs were as follows: 94 °C for 1 min; 32 cycles of 98 °C for 10 s, 68 °C for 3 min; and final elongation for 7 min. PCR conditions used with *wtf18–wtf13* primer pairs were as follows: 94 °C for 1 min; 32 cycles of 94 °C for 30 s, 60 °C for 30 s, and 72 °C for 4 min with a final elongation for 7 min. Junction PCR products were subjected to direct DNA sequencing to map the recombination junction.

Array CGH. Genomic DNA from WT or *sap1-1* revertants was digested with AluI and RsaI. After complete digestion, DNA from WT and *sap1-1* revertants was labeled with Cy-3 dCTP and Cy-5 dCTP, respectively (Amersham Biosciences) using the BioPrime Array CGH Genomic Labeling kit (Invitrogen). Equal amounts of labeled DNA (1.5 μg) were competitively hybridized onto the genome-wide tiling microarray platform (50). Prehybridization, probe hybridization, washing, and drying steps for arrays were performed as for ChIP-chip experiments. The $\log_2$-transformed Cy5/Cy3 ratio is plotted along the chromosome.

Southern Analysis. Genomic DNA was digested with ApaI and DraI for analyzing the subtelomeric repeat and *sap1-1* gene amplification, respectively. The subtelomeric repeat sequence probe was made by digesting pAMP002 with ApaI + EcoRI. Probes for *sap1* and *ade6* were generated by PCR using the primers listed in Table S2.

2D Gel Analysis. *cdc10-V50* and *cdc10-V50 sap1-1* cells were arrested in G1 by incubation at 35 °C for 4 h. After a shift to 25 °C to resume DNA synthesis, 250 mL (OD_{600} ~0.5) were harvested following the addition of 50 mL 200 mM EDTA and 2.5 mL 10% NaN_3. Cells were washed in CSE buffer (1.2 M sorbitol, 20 mM citrate phosphate, 40 mM EDTA), and the cell wall was digested using 0.25 mg/mL Zymolyase 100T (Seikagaku) in CSE buffer for 30 min. Cells were pelleted and resuspended in

CSE buffer. An equal amount of 1% InCert agarose (Cambrex) was added, and cells were embedded into an agarose plug mold, which was digested in solution (10 mM Tris, 1% lauryl sarcosine, 25 mM EDTA, 1 mg/mL Proteinase K) overnight at 50 °C. The digestion solution was removed, followed by incubation in storage buffer (10 mM Tris, 50 mM EDTA) twice for 1 h. DNA agarose plugs were washed three times in Tris/EDTA (TE) buffer and twice in restriction enzyme buffer. DNA plugs were incubated with an appropriate restriction enzyme (40 U per plug) at 37 °C overnight. Agarose was melted by heating to 65 °C for 5 min and to 37 °C for 5 min. An additional 40 U of restriction enzyme was added for 2 h at 37 °C. Digested DNA was separated on a 0.4% agarose gel in Tris/borate/EDTA (TBE) + 3 mM MgCl2 buffer. The first dimension was run at 1.2 V/cm for 21 h at room temperature. The second dimension was run at 6 V/cm for 5 h with buffer circulation at 4 °C through a 0.9% agarose gel in TBE + 3 mM MgCl2 buffer containing 0.4 μg/mL ethidium bromide. Southern transfer and hybridization were carried out using a position-specific *wtf9* probe generated by PCR using the primers listed in Table S2.

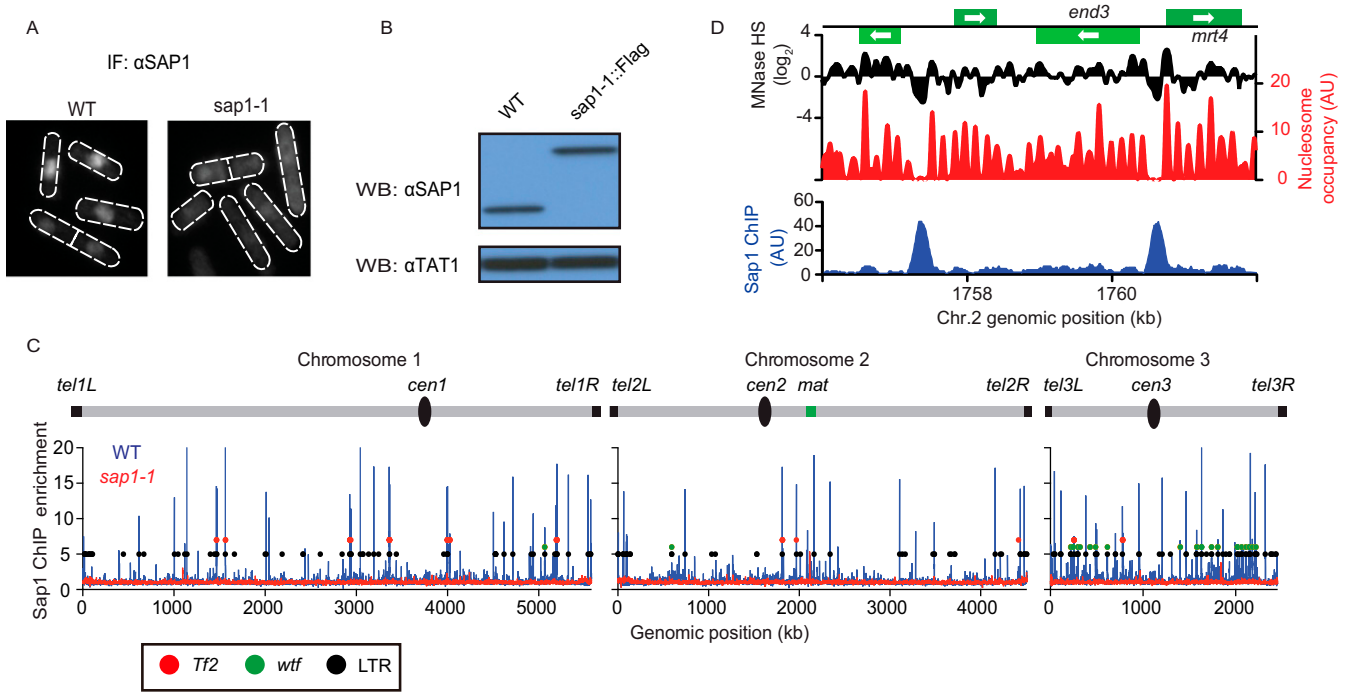

Fig. S1. Sap1 is an abundant nuclear DNA-binding protein and localizes broadly across the genome. (*A*) Subcellular localization of Sap1. Sap1 localizes to the nucleus, whereas the mutant Sap1-1 is diffused throughout the cell. (*B*) The total protein levels of Sap1 and Sap1-1 were determined by Western blot (WB) using anti-Sap1 antibody. TAT1 was used as a loading control. (*C*) ChIP-chip analysis of Sap1 and Sap1-1 protein. Black, green, and red circles indicate the genomic positions of LTR, *wtf*, and *Tf2* elements, respectively. (*D*) ChIP-sequencing analysis of Sap1 [adapted from Zaratiegui et al. (18)] compared with nucleosome occupancy. MNase hypersensitivity mapping data are adapted from our previous study (52). Green bars represent ORFs according to the 2007 *S. pombe* genome assembly.

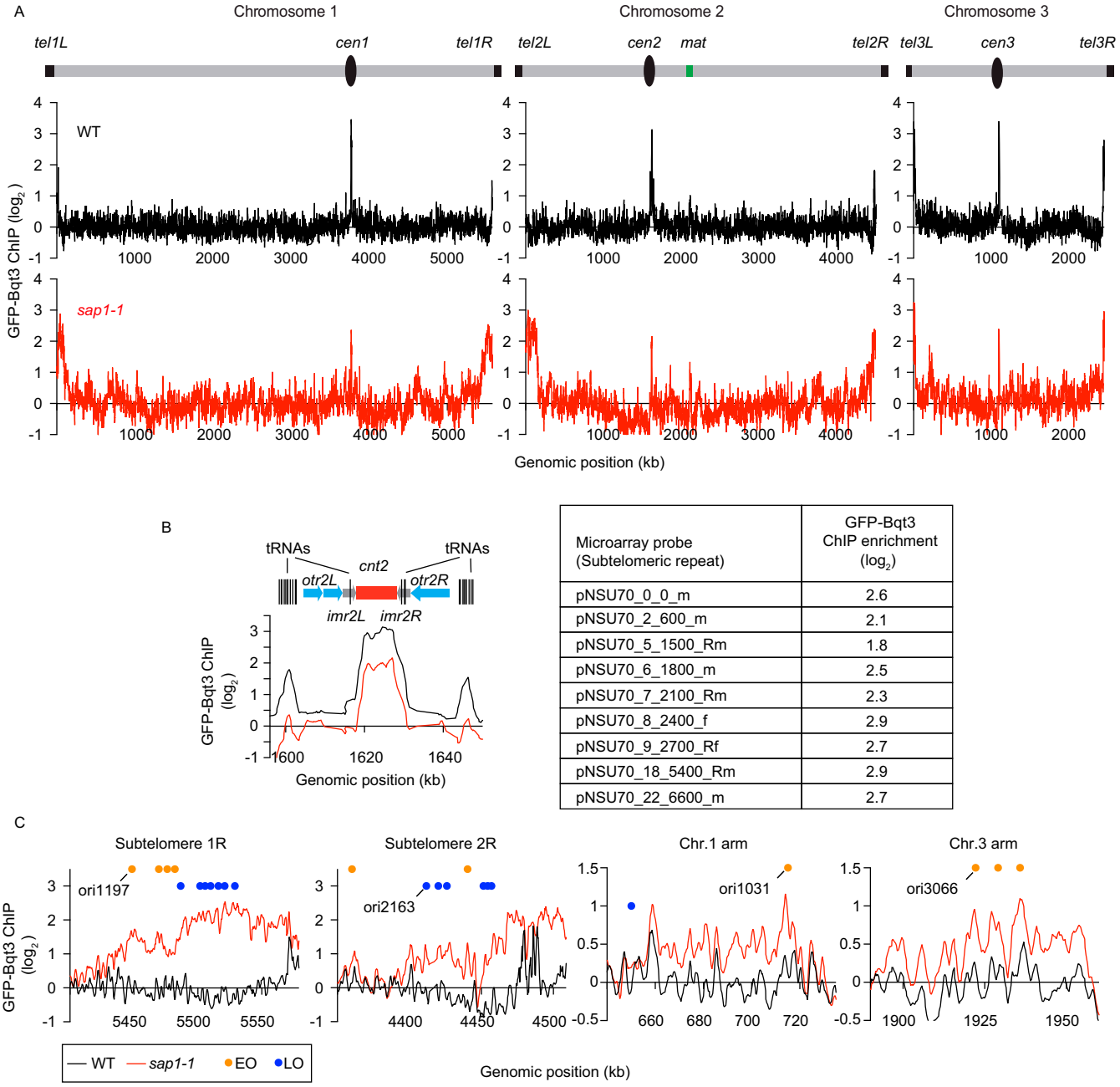

Microarray probe (Subtelomeric repeat)	GFP-Bqt3 ChIP enrichment (log_2)
pNSU70_0_0_m	2.6
pNSU70_2_600_m	2.1
pNSU70_5_1500_Rm	1.8
pNSU70_6_1800_m	2.5
pNSU70_7_2100_Rm	2.3
pNSU70_8_2400_f	2.9
pNSU70_9_2700_Rf	2.7
pNSU70_18_5400_Rm	2.9
pNSU70_22_6600_m	2.7

Fig. S2. *sap1-1* causes a shift in chromosome configuration and allows new genomic contacts to be made with the nuclear membrane. (*A*) Genome-wide GFP-Bqt3 ChIP-chip analysis of WT and *sap1-1* cells. (*B*, *Left*) GFP-Bqt3 ChIP enrichment at centromere 2. The vertical line indicates individual copies of tRNAs; the red box indicates the central core domain (*cnt*); the gray arrows indicate the innermost repeats (*imr*); the blue arrows indicate the outer repeat region (*otr*). (*Right*) GFP-Bqt3 ChIP enrichment at subtelomeric repeats. (*C*) GFP-Bqt3 ChIP enrichment across extended subtelomeric domains and certain chromosome arm regions where new genomic contacts with the nuclear membrane emerge in *sap1-1* cells. Orange and blue circles represent early- and late-replication origins, respectively, as annotated by Hayashi and colleagues (48).

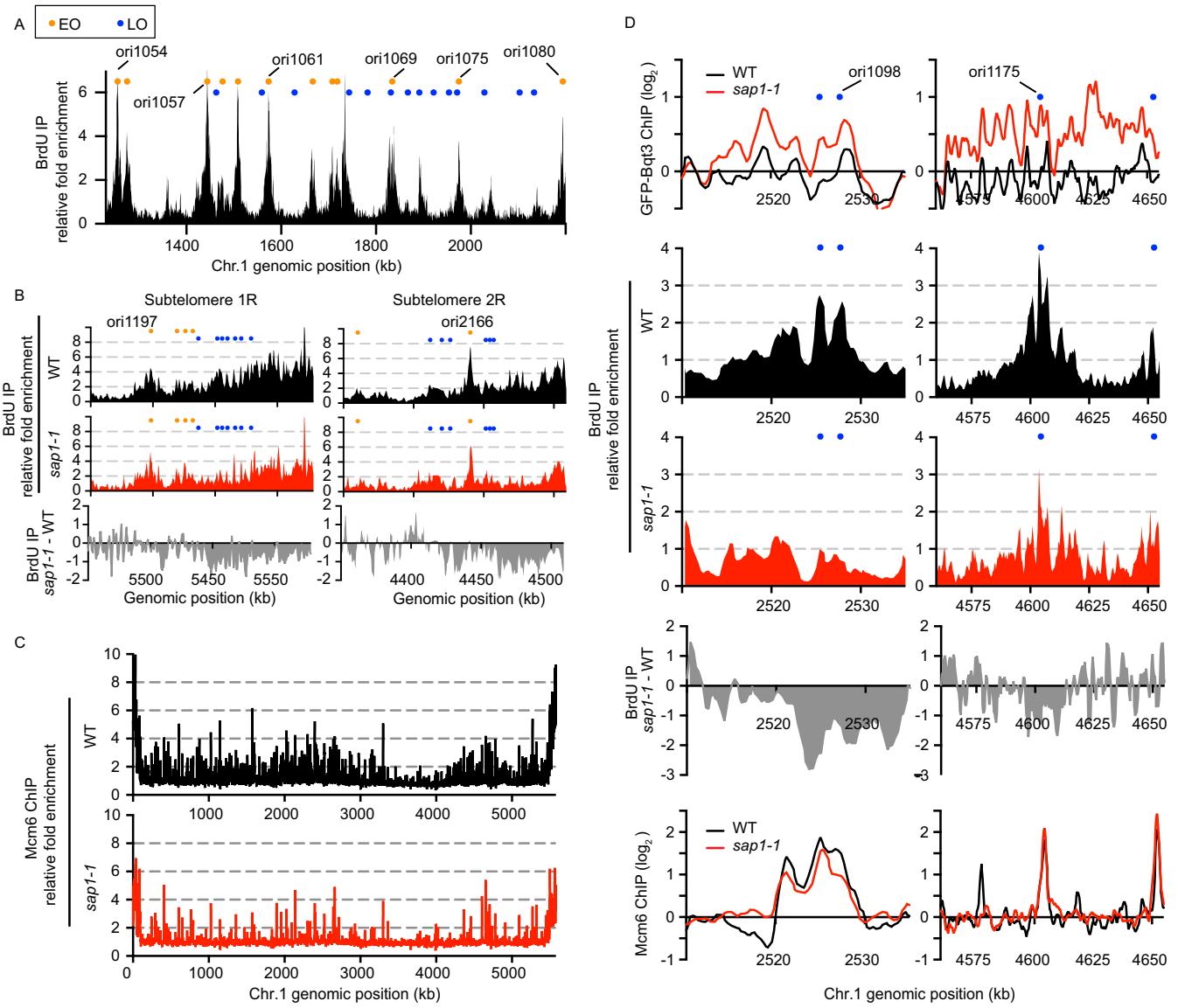

Fig. S3. Replication profiles of WT and *sap1-1* cells. (*A*) Replication profile of a segment of chromosome 1 in WT cells. Detection of early-replication origins in the *cdc10-v50* single-mutant background by BrdU immunoprecipitation. Cells were released from the G1-phase in the presence of HU. (*B*) Replication profiles of subtelomeric regions in WT (*Top*) and *sap1-1* (*Middle*) cells. Cells carrying the *cdc10-v50* allele were arrested and released from G1-phase in the presence of HU. (*Bottom*) The difference between *sap1-1* and WT cells is plotted. Orange and blue circles represent the early- and late-replication origins, respectively, as annotated by Hayashi and colleagues (48). (*C*) Mcm6 ChIP-chip analysis of chromosome 1 in WT and *sap1-1* cells. (*D*) DNA replication profile of chromosome arm regions in WT and *sap1-1* cells. GFP-Bqt3 and Mcm6 ChIP-chip are shown in the top and bottom graphs, respectively. IP, immunoprecipitation.

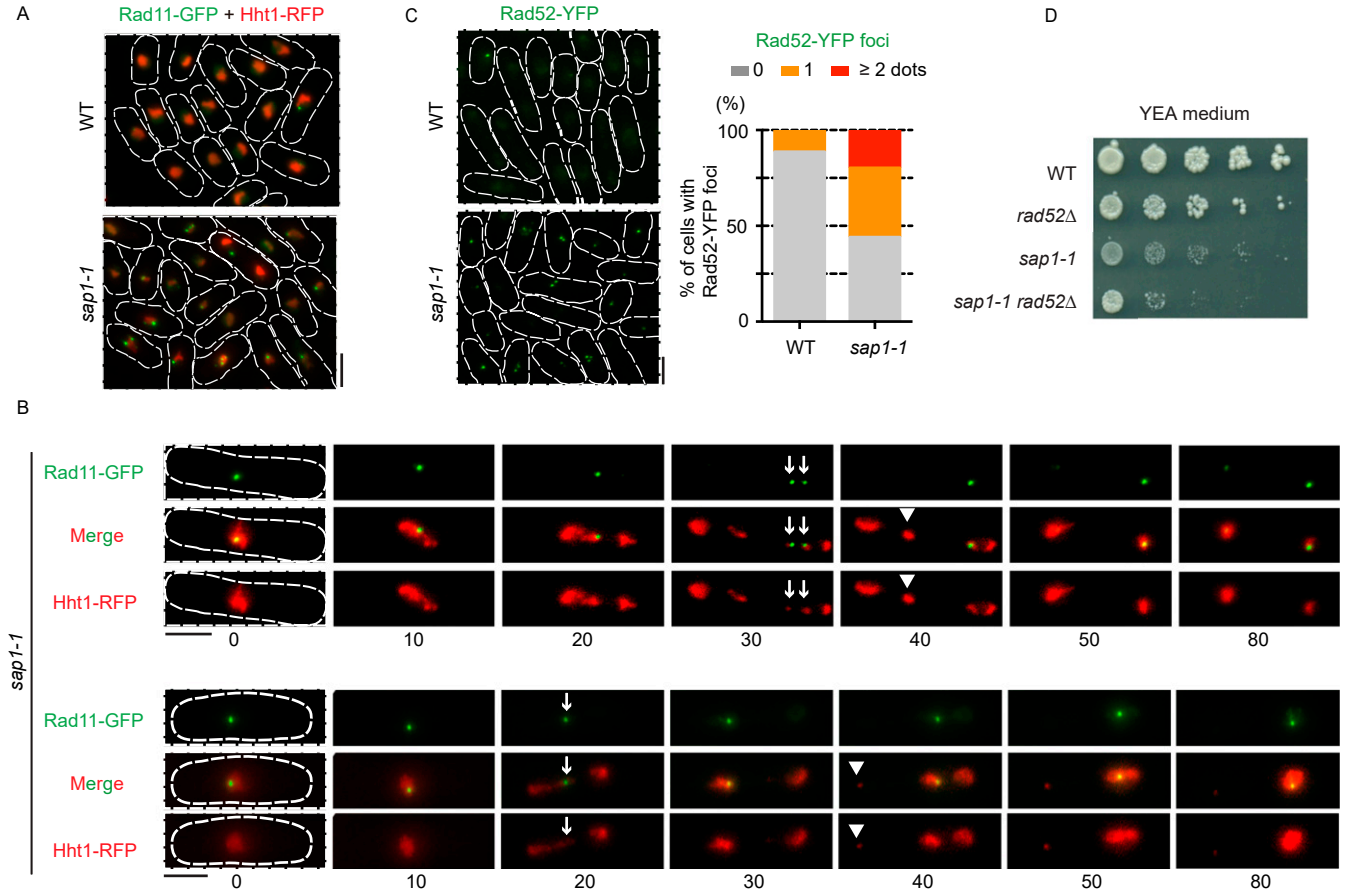

Fig. S4. Replication-associated DNA damage followed by division may cause chromosome fragmentation in *sap1-1* cells. (*A*) The RPA component Rad11-GFP forms discrete foci in *sap1-1* cells. Cells expressing Rad11-GFP (green) and Hht1-RFP (red) were cultured at 26 °C and then were shifted to 33 °C for 6 h. (Scale bar, 5 μm.) (*B*) Time-lapse observation of Rad11-GFP (green) and Hht1-RFP (red) in *sap1-1* cells during M-phase. Projection images of each indicated time point are shown. Numbers below the images indicate the time in minutes. Chromatin (Hht1-RFP) appears fragmented and lags behind during M-phase in *sap1-1* cells (arrowheads). Rad11-GFP is observed near fragmented chromatin masses (arrow). (Scale bars, 5 μm.) (*C*) Rad52 forms nuclear foci in *sap1-1* cells. Cells expressing Rad52-YFP were cultured at 26 °C and then were shifted to 33 °C for 6 h. The percentage of mononuclear cells with Rad52-YFP foci ($n = 84$ for WT cells and $n = 103$ for *sap1-1* cells) is shown. (Scale bar, 5 μm.) (*D*) Fivefold serial dilution assay of indicated strains on complete medium at 30 °C.

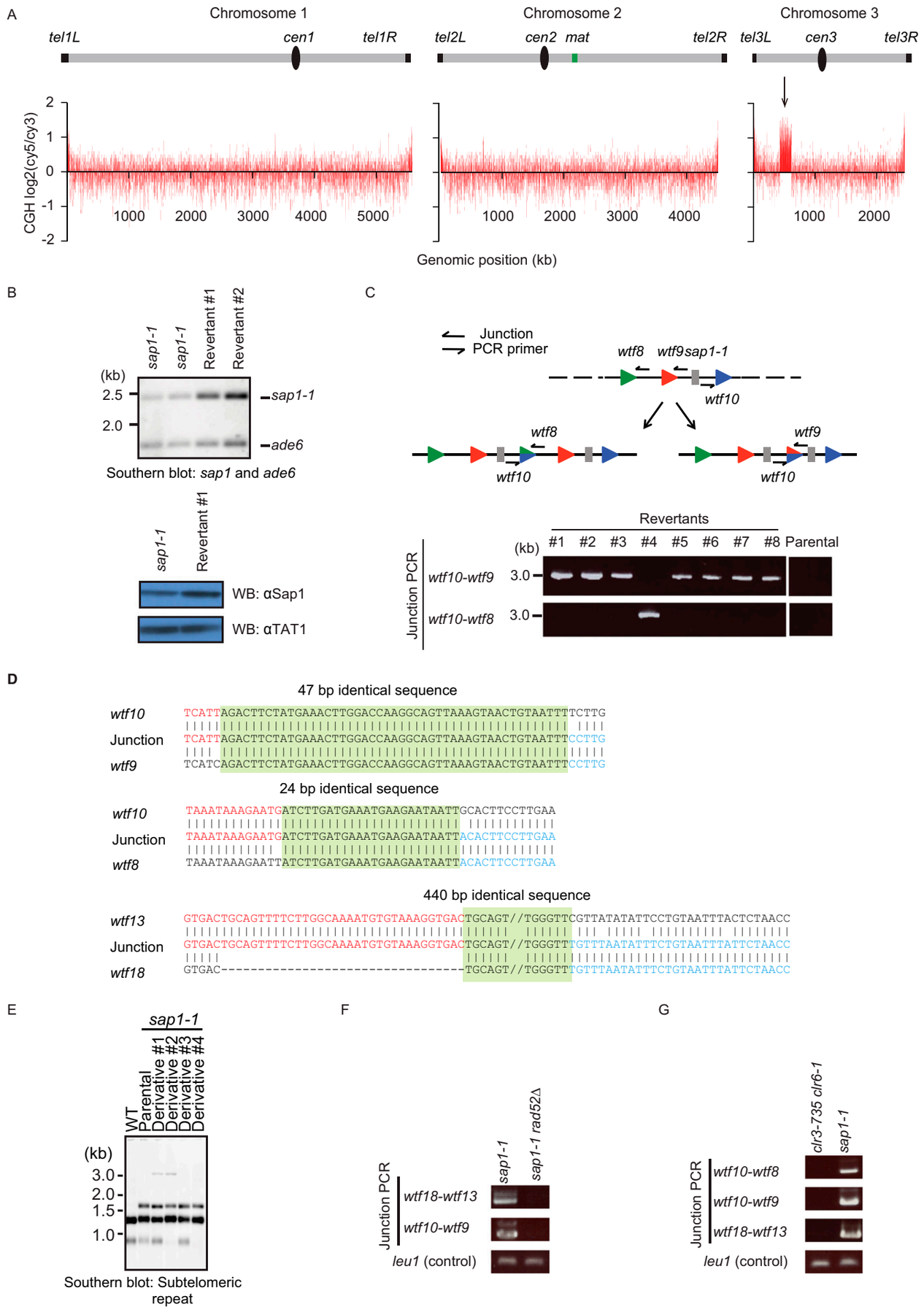

Fig. S5. Repeat structures, including *wtf*s, are destabilized in *sap1-1* cells. (*A*) Microarray CGH analysis of revertants reveals a copy number gain of a region encompassing the *sap1-1* locus on chromosome 3 (arrow). (*B*) The genomic alteration was confirmed by Southern blot analysis. A mixture of *sap1* and *ade6* probes was used for southern hybridization. Both *sap1* and *ade6* genes map to chromosome 3, but *ade6* is located outside of the copy number gain region. The *sap1-1* signal is higher in the revertants than in the parental *sap1-1* strain. The *ade6* locus was used as a loading control. (*Lower*) Western blot analysis of whole-cell lysates prepared from *sap1-1* cells and a revertant with a *sap1-1* duplication. The duplication results in the increased total protein level of Sap1-1. TAT1 was used as a loading control. (*C*) Junction PCR was used to determine that the copy number gain results from direct tandem-oriented duplication. All revertants contained a common copy number gain ~100- to 150-kb in size. (*D*) Rearrangements are mediated by the 47- to 440-bp identical DNA sequence in *wtf* elements (highlighted in green). Junction PCR products were subjected to Sanger DNA sequencing to map the recombination junction. (*E*) Southern blot analysis of ApaI-digested genomic DNA using the subtelomeric repeat sequence probe. *sap1-1* cells were cultured at the semipermissive temperature, and genomic DNA was isolated from independent colonies (derivatives). (*F*) Junction PCR analysis of *wtf*-mediated recombination in a strain lacking the HR factor Rad52. (*G*) Junction PCR analysis of *wtf*-mediated recombination in a strain expressing mutant Clr3 and Clr6 HDAC proteins (*clr3-735 clr6-1*), which have been implicated in the repression of *wtf*.

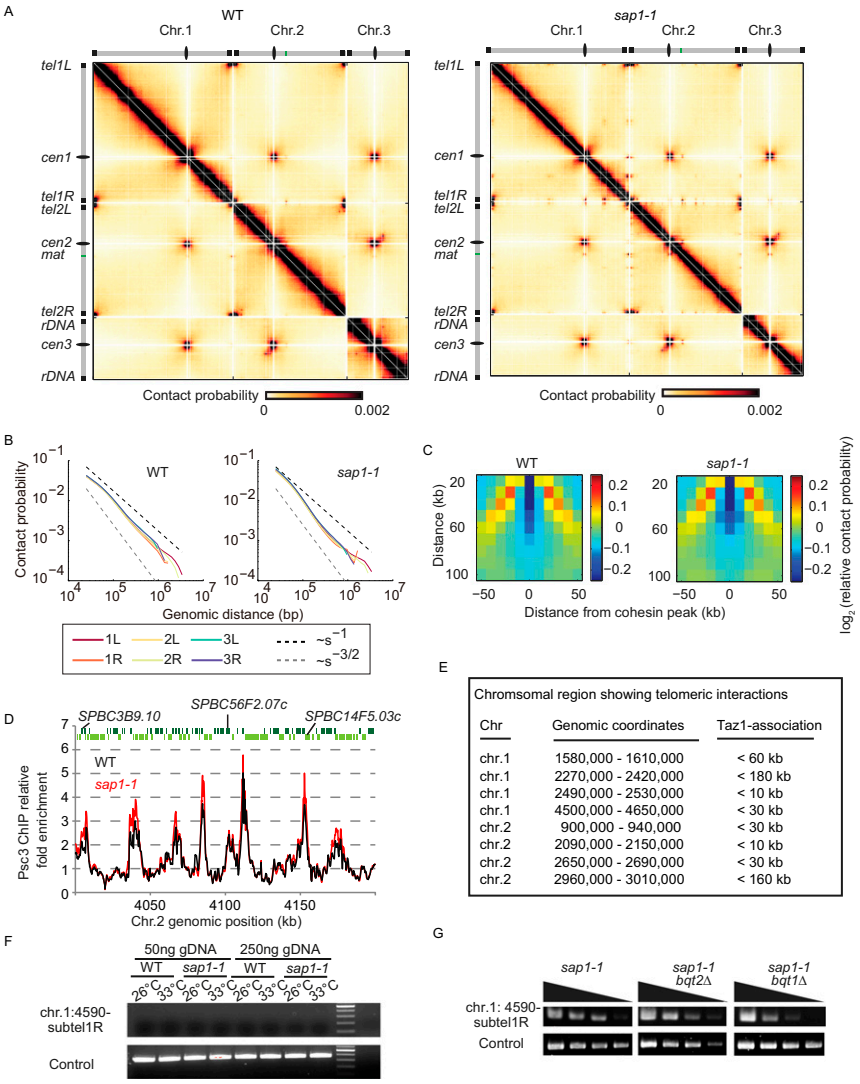

Fig. S6. Fundamental features of *S. pombe* genome organization are preserved in *sap1-1* cells. (*A*) Genome-wide Hi-C heatmaps for WT and *sap1-1* cells at 10-kb resolution. WT data are adapted from Mizuguchi et al. (8). (*B*) Contact probability as a function of genomic distance for different chromosomal arms. The decay of intra-arm contact probability as a function of genomic distance, plotted for each chromosome arm. Contact probability *P(s)* values decrease more slowly at short distances. The black and gray dashed lines represent the slope for fractal globules (−1) and polymers in a melt (−3/2), respectively. (*C*) Relative probability of contact around a cohesin peak as a function of insulation distance averaged over all cohesin peaks (insulation plot). Contact frequency between regions separated by cohesin peaks was depleted in both WT and *sap1-1* cells. (*D*) Cohesin (Psc3-GFP) ChIP-chip data of a segment of chromosome 2 in WT and *sap1-1* cells. The binding profile of cohesin is unaffected in *sap1-1* cells. (*E*) The regions of chromosome arms in which new interactions emerge in *sap1-1* cells. Distances from the center of the new Hi-C interaction region to the nearest Taz1 ChIP enrichment are shown. (*F*) Genomic DNA isolated from WT and *sap1-1* cells was analyzed using the 3C PCR primer. WT and mutant strains were initially cultured at 26 °C and then were shifted to 33 °C for 6 h. (*G*) 3C PCR analysis of a *sap1-1*–specific interaction (chr.1: 4,590-kb region and subtelomere 1R) in *sap1-1 bqt1Δ* and *sap1-1 bqt2Δ* cells.

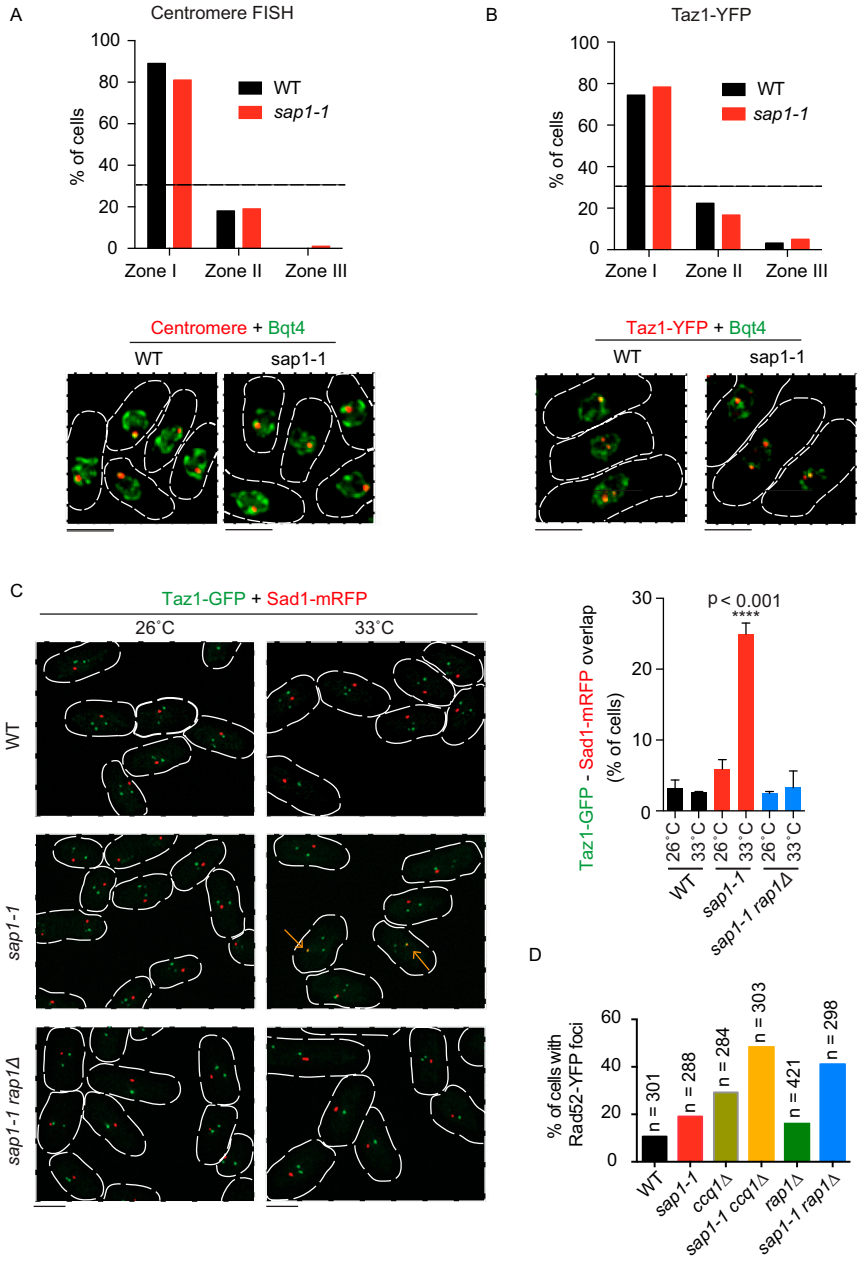

Fig. S7. Shelterin facilitates specific interactions in *sap1*-mutant cells. (*A*) Nuclear peripheral localization of centromeres in WT and *sap1-1* cells. The shortest 2D distance between the centromere FISH signal (pRS140) and the NE (GFP-Bqt4) in the focal plane near the nuclear midplane was measured and classified as zone I (nuclear periphery, 0–0.22 μm from the NE), zone II (middle, 0.23–0.51 μm from the NE), or zone III (nuclear interior, 0.52–1.20 μm from the NE). (n = 107 for WT, and n = 101 for *sap1-1* cells). The dashed line at 33% corresponds to random distribution. (*B*) Nuclear peripheral localization of Taz1-YFP (telomeres) in WT and *sap1-1* cells. The shortest 2D distance between Taz1-YFP and the NE (GFP-Bqt4) in the focal plane near the nuclear midplane was measured and classified into three zones (n = 94 for WT and n = 166 for *sap1-1* cells). The dashed line at 33% corresponds to random distribution. (*C*, *Right*) Graph of the percentage of mononuclear cells showing colocalization of telomeres (Taz1-GFP) and SPB (Sad1-mRFP). WT and mutant strains were initially cultured at 26 °C and then were shifted to 33 °C for 6 h. ****$P \leq 0.0001$ (two-tailed Mann–Whitney test). Two independent experiments; total n = 207 (26 °C, WT), n = 299 (33 °C, WT), n = 198 (26 °C, *sap1-1*), n = 207 (33 °C, *sap1-1*), n = 328 (26 °C, *sap1-1 rap1Δ*), n = 288 (33 °C, *sap1-1 rap1Δ*). (*Left*) Time-lapse images were recorded at 30-s intervals for 3 min. Associations were determined by codirectional movement and colocalization. Representative images of indicated strains are shown. Arrows indicate telomere–SPB association. (*D*) Cells expressing Rad52-YFP were cultured at 26 °C and then were shifted to 33 °C for 6 h. The percentage of mononuclear cells with Rad52-YFP foci is shown. n, total number of cells examined for each strain. (Scale bars, 5 μm in *A*–*C*.)

Table S1. Correlation of Bqt3-enriched sites with DNA replication origins in *sap1-1* cells

Chromosome	Start	End	RO
Chr.1	9,511	180,335	1E, 12L
	198,008	206,219	1E
	237,586	334,267	4L
	406,770	424,189	1L
	653,884	721,267	1E
	758,940	816,430	4L
	1,016,329	1,037,794	1L
	1,786,864	1,814,871	—
	1,946,262	1,965,065	3L
	2,173,436	2,199,069	1E
	2,388,787	2,431,246	2L
	2,467,949	2,529,844	3E
	2,748,839	2,780,767	1E
	3,508,187	3,580,218	5E
	3,672,524	3,702,244	1E
	3,811,877	3,844,767	1E
	4,564,577	4,669,494	2L
	4,947,488	5,004,398	1E, 1L
	5,176,441	5,579,133	7E, 10L
Chr.2	0	175,219	5E, 12L
	189,553	212,916	2L
	270,929	335,118	5E
	831,874	841,287	3E
	1,856,436	1,875,286	1L
	3,689,923	3,808,809	2E, 3L
	4,109,417	4,150,350	1L
	4,306,404	4,539,804	2E, 7L
Chr.3	183,232	262,188	4E
	296,941	327,165	1E
	425,464	454,774	—
	594,129	606,341	1E
	628,586	655,000	1E
	1,232,865	1,286,587	1E
	1,338,386	1,346,168	1E
	1,366,120	1,373,576	2E
	1,399,462	1,419,415	2E
	1,489,136	1,563,970	4E
	1,892,334	1,975,624	4E
	2,196,017	2,241,338	1E
	2,196,149	2,433,690	5E, 1L

The 2007 *S. pombe* genome assembly was used for start and end coordinates of regions. E, Early origin; L, late origin; RO, replication origin.

Table S2. Primers used in this study

Use	Name	Sequence
ChIP	*rtn1*	5′-CGATGCCATACTCCCATCTC-3′; 5′-TCATCTCATTATGCGTTGTGTG-3′
	Tf2-12	5′-GCATGTCTGTTACCTTTGCT-3′; 5′-CCTTTTTCCTAAAAGGAGTTAAT-3′
	wtf9/LTR	5′-TCACCAATGCAGAGAAGCTG-3′; 5′-TCACCGCAGTTCTACGTATCC-3′
	leu1 (control)	5′-TTTGGTCAAGAGCCCTCGTA–3′; 5′-TAGAAGCCTCACCTCCCAAA-3′
FISH	*rtn1 #1*	5′-AGGTAGAGAAACTGCAAGAGGTGT-3′; 5′-CTAGGCAAAGGAAGAGAGCTAAGAG-3′
	rtn1 #2	5′-CTCCTGCTTCTCCTAACACCTCTAT-3′; 5′-GAGTCCATCAAGCAGGTTTCTAGT-3′
Southern	*sap1*	5′-ACTATACACCACTCTTCC-3′; 5′-AATAGAAGCAACCCAACTAGCG-3′
	ade6	5′-CGGTGCAACTTTGCATCTTTATGG–3′; 5′-AATTCATCTAAAATGACGGCAGC-3′
2D gel	*wtf9 2D*	5′-TGTTTCAAGGCAATGAGCTG-3′; 5′-ACGGGCTAGCTGATCTTCAA-3′
Junction PCR	*wtf10-wtf8*	5′-CGCTTTTCCAATTCGTCAAT-3′; 5′-TATGAAAGAGCACGGCGAGT-3′
	wtf10-wtf9	5′-CGCTTTTCCAATTCGTCAAT-3′; 5′-GACTTCGGTCCTCAATGCAC–3′
	wtf18-wtf13 F	5′-CCCTTCTTATTCACCCCAAC-3′; 5′-CGCAAAACGATCATTTCCTT-3′
	leu1 (control)	5′-TTTGGTCAAGAGCCCTCGTA-3′; 5′-TAGAAGCCTCACCTCCCAAA-3′
3C	*3C control*	5′-CAAGCACGAAGTCGTAGGCGTTTTTCAGAG-3′; 5′-CATACGACGCCTTGGACGATGTCGATTCAT-3′
	chr.1: 4,590-subtel1R	5′-TGCGTCAAACAAGGACTATCCTGATCGC-3′; 5′-ACCCGGACTATATGTTCCAGAAGAAGACG-3′

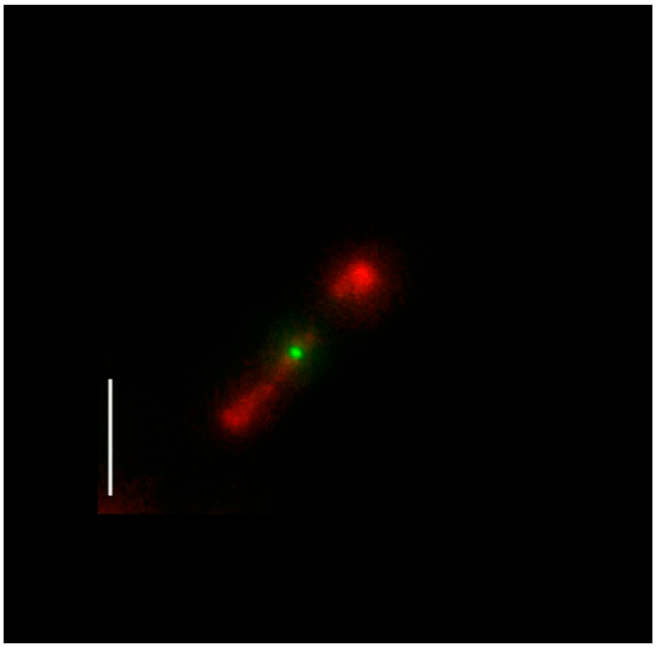

Movie S1. Live-cell imaging of Rad11 foci in *sap1-1* cells through mitosis (example 1). Time-lapse microscopy of a representative cell shows chromosomes during M-phase as revealed by the red RFP-tagged histone, Hht1-RFP. A discrete Rad11-GFP green focus is observed near the fragmented chromatin masses in *sap1-1*. Cells were imaged on a DeltaVision Elite microscope (GE Healthcare) with a 100× 1.4 NA Plan Super Apochromat oil lens (Olympus) using SoftWoRX 6.0.

Movie S1

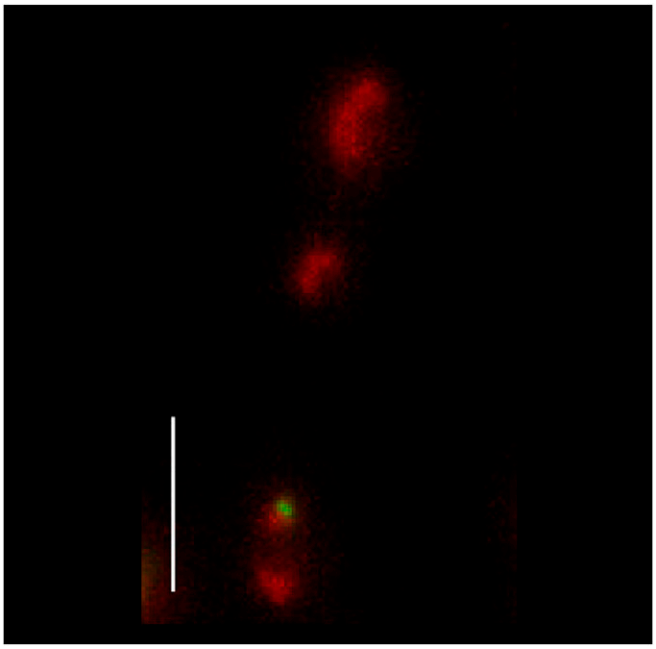

Movie S2. Live-cell imaging of Rad11 foci in *sap1-1* cells through mitosis (example 2). Time-lapse microscopy showing chromosomes marked by red RFP-tagged histone, Hht1-RFP, during M-phase. Cells were imaged on a DeltaVision Elite microscope (GE Healthcare) with a 100× 1.4 NA Plan Super Apochromat oil lens (Olympus) using SoftWoRX 6.0.

Movie S2

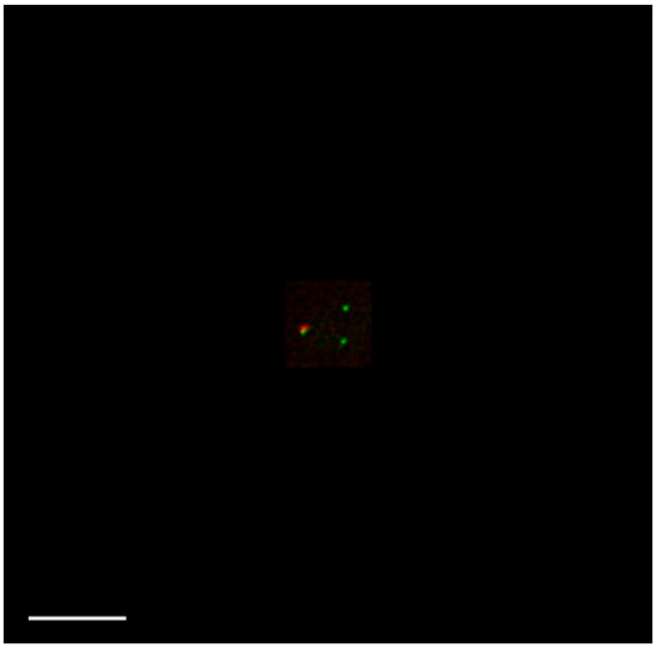

Movie S3. Centromere and telomere localization in *sap1-1* cells (example 1). Time-lapse microscopy of a representative cell reveals continual overlap of centromeres (marked by red Sad1-RFP) and telomeres (marked by green Taz1-GFP) in *sap1-1*. Cells were imaged on a DeltaVision Elite microscope (GE Healthcare) with a 100× 1.4 NA Plan Super Apochromat oil lens (Olympus) using SoftWoRX 6.0.

Movie S3

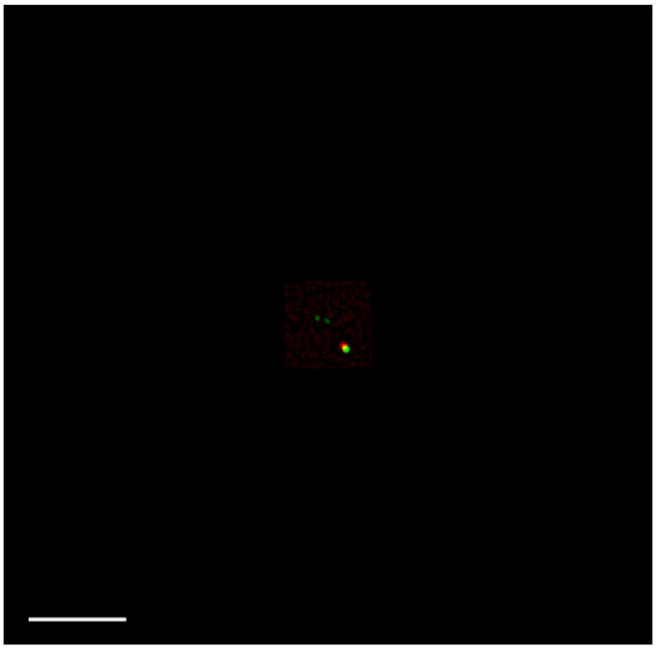

Movie S4. Centromere and telomere localization in *sap1-1* cells (example 2). Time-lapse microscopy of a *sap1-1* cell showing continual overlap of Sad1-RFP (centromeres) and Taz1-GFP (telomeres). Cells were imaged on a DeltaVision Elite microscope (GE Healthcare) with a 100× 1.4 NA Plan Super Apochromat oil lens (Olympus) using SoftWoRX 6.0.

Movie S4

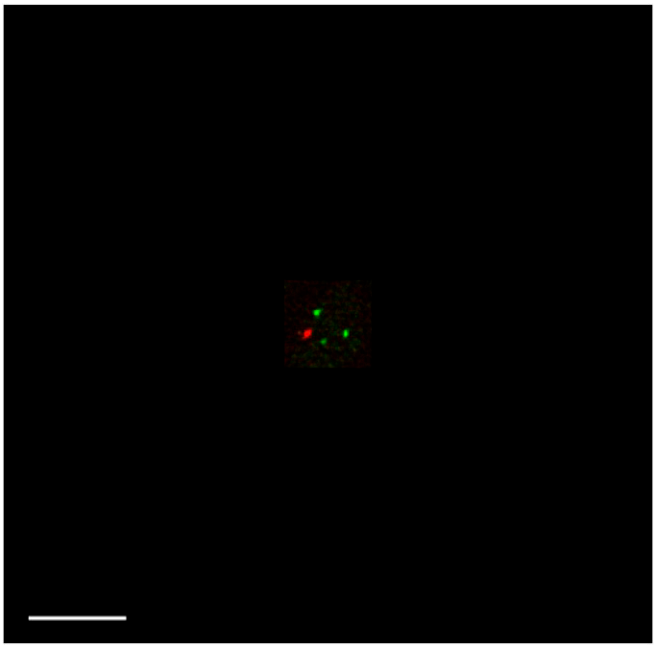

Movie S5. Centromere and telomere localization in WT cells (example 1). Time-lapse microscopy of a representative WT cell, in which continual overlap of centromeres (marked by red Sad1-RFP) and telomeres (marked by green Taz1-GFP) is not observed. Cells were imaged on a DeltaVision Elite microscope (GE Healthcare) with a 100× 1.4NA Plan Super Apochromat oil lens (Olympus) using SoftWoRX 6.0.

Movie S5

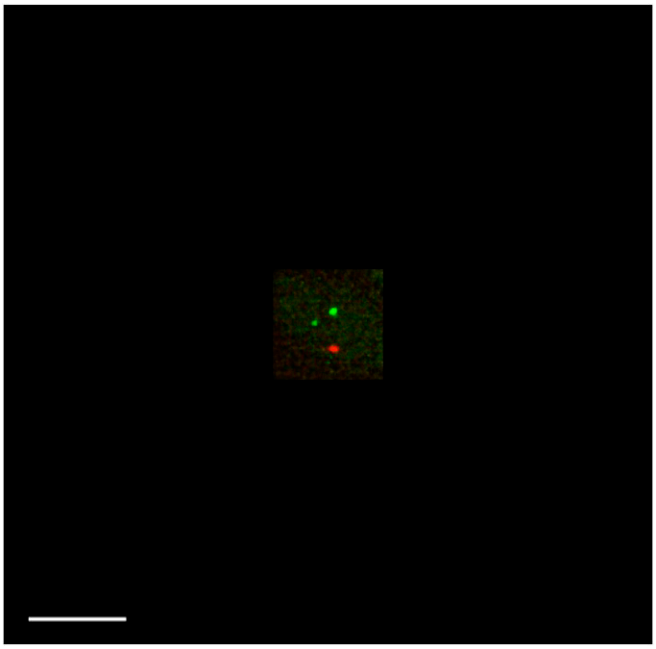

Movie S6. Centromere and telomere localization in WT cells (example 2). Time-lapse microscopy showing a lack of any continual overlap of Sad1-RFP–marked centromeres and Taz1-GFP telomeres. Cells were imaged on a DeltaVision Elite microscope (GE Healthcare) with a 100× 1.4 NA Plan Super Apochromat oil lens (Olympus) using SoftWoRX 6.0.

Movie S6